RESEARCH ARTICLE | APRIL 09 2024

## Interfacial exchange dynamics of biomolecular condensates are highly sensitive to client interactions *⊙*

Ushnish Rana <sup>®</sup>; Ned S. Wingreen <sup>®</sup>; Clifford P. Brangwynne <sup>®</sup>; Athanassios Z. Panagiotopoulos **№** <sup>®</sup>



J. Chem. Phys. 160, 145102 (2024)

https://doi.org/10.1063/5.0188461

A CHORUS





### Articles You May Be Interested In

Liquid state theory study of the phase behavior and macromolecular scale structure of model biomolecular condensates

J. Chem. Phys. (July 2023)

Stability and deformation of biomolecular condensates under the action of shear flow

J. Chem. Phys. (June 2024)

Emerging experimental methods to study the thermodynamics of biomolecular condensate formation

J. Chem. Phys. (March 2024)





# Interfacial exchange dynamics of biomolecular condensates are highly sensitive to client interactions

Cite as: J. Chem. Phys. 160, 145102 (2024); doi: 10.1063/5.0188461 Submitted: 21 November 2023 • Accepted: 22 March 2024 • Published Online: 9 April 2024







Ushnish Rana, 1 D Ned S. Wingreen, 2 Clifford P. Brangwynne, 1,3,4 D

### **AFFILIATIONS**

- Department of Chemical and Biological Engineering, Princeton University, Princeton, New Jersey 08544, USA
- <sup>2</sup>Lewis-Sigler Institute for Integrative Genomics and Department of Molecular Biology, Princeton University, Princeton, New Jersey 08544, USA
- <sup>3</sup>Howard Hughes Medical Institute, Chevy Chase, Maryland 20815, USA

and Athanassios Z. Panagiotopoulos<sup>1,a)</sup>

- Omenn-Darling Bioengineering Institute, Princeton University, Princeton, New Jersey 08544, USA
- a) Author to whom correspondence should be addressed: azp@princeton.edu

### **ABSTRACT**

Phase separation of biomolecules can facilitate their spatiotemporally regulated self-assembly within living cells. Due to the selective yet dynamic exchange of biomolecules across condensate interfaces, condensates can function as reactive hubs by concentrating enzymatic components for faster kinetics. The principles governing this dynamic exchange between condensate phases, however, are poorly understood. In this work, we systematically investigate the influence of client–sticker interactions on the exchange dynamics of protein molecules across condensate interfaces. We show that increasing affinity between a model protein scaffold and its client molecules causes the exchange of protein chains between the dilute and dense phases to slow down and that beyond a threshold interaction strength, this slowdown in exchange becomes substantial. Investigating the impact of interaction symmetry, we found that chain exchange dynamics are also considerably slower when client molecules interact equally with different sticky residues in the protein. The slowdown of exchange is due to a sequestration effect, by which there are fewer unbound stickers available at the interface to which dilute phase chains may attach. These findings highlight the fundamental connection between client–scaffold interaction networks and condensate exchange dynamics.

Published under an exclusive license by AIP Publishing. https://doi.org/10.1063/5.0188461

### I. INTRODUCTION

Phase separation of proteins and nucleic acids has emerged as a new biophysical paradigm for the organization of biological macromolecules inside living cells.<sup>1–3</sup> Extensive work has established that the formation of these biological condensates is driven by the phase separation of multivalent proteins, which are closely analogous to associative polymers.<sup>4,5</sup> These proteins, often harboring intrinsically disordered regions,<sup>6,7</sup> contain multiple residues or domains, which can form a network of noncovalent bonds driving the formation of a dense phase.<sup>8</sup> These residues or sequence motifs, often termed "stickers,"<sup>9,10</sup> typically interact through short-ranged interactions mediated by aromatic residues and also hydrophobic or electrostatic interactions.<sup>11,12</sup> However, while these multivalent proteins

usually act as the primary scaffolds for biomolecular phase separation, condensates are often enriched in "client" molecules,  $^{13}$  which have favorable interactions with the multivalent proteins but cannot phase separate on their own. Thus, condensates often feature a rich network of interactions whose overall composition regulates their material and functional properties.  $^{14-18}$ 

The ability of biomolecular condensates to concentrate client species is widely accepted to be critical to their biological function. In many cases, clients are biomolecules with enzymatic activity, which are spatially concentrated by condensates to potentially enable more efficient reactions or perform regulatory functions. <sup>19–22</sup> Furthermore, condensates allow selective yet rapid exchange of biomolecules across their interfaces, which is most likely critical for their ability to spatiotemporally organize biomolecules within cells.

As an example, diffusive fluxes across interfaces have been shown to provide a mechanism of size regulation in an active condensate. <sup>23,24</sup> Similarly, fluxes of regulatory biomolecules such as kinases and phosphatases offer a compelling mechanism for the active formation and dissolution of condensates. <sup>25,26</sup> There has been growing interest in deciphering how biomolecular interaction networks tune the equilibrium assembly of multicomponent condensates. <sup>27–30</sup> Recently, there has been great interest in understanding the organization and dynamics of condensate interfaces. Condensate interfaces have been shown to display rich phenomenology ranging from modulating redox reactions to promoting the growth of amyloid fibrils. <sup>31,32</sup> Computational investigations of biological condensates have also explored the organization and conformations of scaffold molecules at these interfaces. <sup>33,34</sup>

Molecular dynamics simulations with coarse grained protein models have emerged as a powerful tool for investigating the physicochemical principles behind the formation of biological condensates. 35,36 Residue-level models, where each amino acid is modeled as a single bead, have proven highly successful in explaining protein condensate phase behaviors including sequence-dependent properties and multicomponent organization 37-40 at a reasonable computational cost. Although residue-level models more closely approximate real systems, minimal sticker-spacer9 or hydrophobicpolar models<sup>41,42</sup> with two bead types have proven to be highly effective at efficiently probing the biophysical principles underlying condensate formation. Recent work utilizing a minimal coarse-grained model has suggested that condensate interfaces might impose strong transport resistance to fluxes across them, 43 a finding indirectly suggested by experimental measurements.44 While previous work has investigated this question for simple, one-component condensates, it is unclear how the presence of protein scaffolds-mediated by a complex network of interactions—and their clients would influence the dynamics of fluxes across condensate interfaces.

In this work, we investigate how the presence of client molecules can influence the dynamics of exchange across condensate interfaces. Utilizing molecular dynamic simulations with a minimal model of a phase-separating protein with interacting clients, we characterize the effects of stoichiometry and interaction strength on exchange dynamics. Furthermore, we investigate the role of interaction network symmetry, demonstrating that differences in interaction strength between the client and different sticky residues can change the condensate's dynamics. Finally, we explore how the sequestration of stickers by client molecules leads to the slowing of condensate exchange dynamics.

#### II. MODEL AND METHODS

We utilize a coarse-grained sticker-spacer model, which has been used previously to study the phase separation of disordered proteins in the absence of client molecules. The model represents disordered proteins as polymers composed of two types of sticky beads, A and B, which have heterotypic (A–B) attractive interactions implemented through a pair potential with a distance cutoff at  $r=r_0$ . Client-like species were modeled as a third bead-type C, which also has heterotypic interactions with stickers A and B through the same attractive potential function but with differing strengths, as shown in Fig. 1(a):

$$U_a(r) = \begin{cases} -\frac{1}{2} U_{ab} \left( 1 + \cos \frac{\pi r}{r_0} \right), & r \le r_0, \\ 0, & r > r_0. \end{cases}$$
 (1)

We note here that clients can bind to either sticker A or B but also to an A–B sticker pair, thus clients can potentially stabilize sticker–sticker bonds. Physically, this models multivalent clients that feature distinct interaction interfaces for different stickers. Furthermore, to ensure one-to-one binding of stickers, the self-interaction of A–A, B–B, and C–C beads was modeled with a purely repulsive Weeks–Chandler–Andersen interaction, <sup>47</sup>

$$U_r(r) = \begin{cases} 4\epsilon_0 \left[ \left( \frac{\sigma}{r} \right)^{12} - \left( \frac{\sigma}{r} \right)^6 \right] + \epsilon_0, & r \le 2^{1/6} \sigma, \\ 0, & r > 2^{1/6} \sigma. \end{cases}$$
 (2)

Sticker beads were connected by flexible finite extensible nonlinear elastic bonds, which implicitly represent spacers,

$$U_b(r) = -\frac{1}{2}KR_0^2 \ln\left[1 - \left(\frac{r}{R_0}\right)^2\right]. \tag{3}$$

Following previous work,<sup>43</sup> parameters were set as follows:  $K = 0.15k_{\rm B}T/{\rm nm^2}$ ,  $R_0 = 10$  nm,  $U_{\rm ab} = 14k_{\rm B}T$ ,  $r_0 = 1$  nm,  $\epsilon_0 = 1k_{\rm B}T$ , and  $\sigma = 2$  nm. Parameters chosen for the repulsive interaction were found to be sufficient to prevent many-to-one binding of the stickers. For client–sticker cross-interactions  $U_{\rm bc}$  and  $U_{\rm ac}$ , a range of interaction strengths between 1 and  $4k_{\rm B}T$  was considered. For all parameter regimes studied, we observed the formation of equilibrium dense and dilute phases rather than system-spanning networks.<sup>5,48</sup> Since the two sticker beads A and B are thermodynamically identical, we considered a case where client C interacts

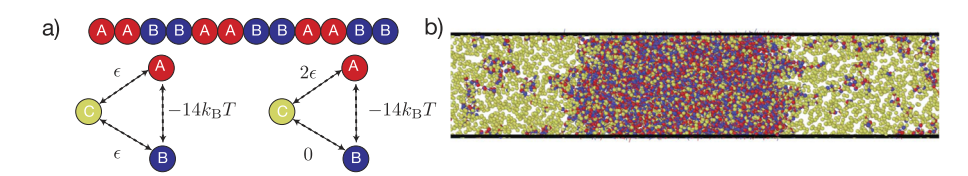


FIG. 1. (a) Schematic showing the model sequence  $(A_2B_2)_3$  and the interaction networks between sticker and client beads for both the symmetric and asymmetric interactions between client C and the two sticker beads A and B. (b) A representative snapshot of a simulation box comprising 1000  $(A_2B_2)_3$  polymers and 12 000 C client beads at coexistence conditions showing a polymer-rich dense phase and a polymer-lean dilute phase. Simulation snapshots were generated using OVITO.

symmetrically with both A and B as well as when it interacts asymmetrically while preserving the same sum of interaction energies. The overall interaction energy was kept constant to ensure equal partition coefficients of the clients between the two cases.

All simulations were performed using the HOOMD-blue simulation package. <sup>49</sup> The equations of motion were integrated using the velocity Verlet algorithm with a time step of  $\delta t = 0.1$  ns. A weakly coupled Langevin thermostat was used with a friction coefficient  $\gamma = 11\,320$  amu/ps and all beads having mass m = 188.5 amu, leading to a damping factor  $\tau = m/\gamma = 10$  ns. We also tested different values of the damping factor and found that our results were robust to this parameter value, as shown in Fig. S1 in the supplementary material. Simulations were run on single Nvidia A100 Graphics Processing Units.

In this work, we consider only a single reference sequence  $(A_2B_2)_3$  in the presence of client molecules. Unless otherwise mentioned, simulations were performed with equal mole fractions of client and stickers. For obtaining coexistence properties, direct coexistence simulations were performed in an extended periodic simulation box of size  $500 \times 50 \times 50$  nm³, as shown in Fig. 1(b). Simulations were initialized by placing a rectangular slab of polymer chains within the region -50 nm < x < 50 nm, while client molecules were placed uniformly outside this region. The system was then equilibrated by performing an NVT run for  $2 \times 10^8$  time steps with a step size of  $\delta t = 0.1$  ns. This was found to be sufficient for establishing equilibrated dense and dilute phases. After equilibration, a production run was performed for another  $2 \times 10^8$  time steps, with simulation snapshots recorded every  $2.5 \times 10^5$  time steps.

To estimate the exchange dynamics of chains between the dilute and dense phases, we utilized an approach described in a recent study. <sup>43</sup> Briefly, chains initially starting out in the dilute phase were labeled and tracked over the course of the simulation, as illustrated in Fig. 2(a). For each frame of the trajectory, labeled chains were checked to see if they remained in the dilute phase or had been associated with the dense phase. A labeled chain was considered to be associated with the dense phase if it was connected by at least one

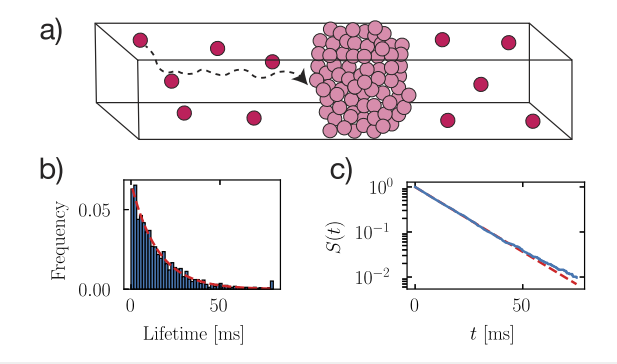


**FIG. 2.** (a) Schematic illustrating the method for estimating the lifetime of a chain in the dilute phase. Individual polymer molecules that were initially in the dilute phase are tracked until they become part of the dense phase for a sufficient duration. (b) The individual chain lifetimes in the dilute phase were recorded on a histogram and found to follow an exponential distribution. (c) Survival probability S(t) is defined as the fraction of labeled chains that remain in the dilute phase. The solid blue curve is the simulated survival probability of dilute phase chains, while the dashed red line is an exponential fit to the data.

sticker-sticker bond to the largest cluster in the simulation box (with a "cluster" defined as a set of chains connected by sticker-sticker bonds). If labeled chains remained associated with the dense phase for "sufficiently long," they were considered to have stably attached. Here, the criterion for sufficiently long attachment was considered to be 40 consecutive snapshots, i.e., 1 ms. The timescale of chain exchange between phases was then estimated by fitting an exponential distribution to the fraction of labeled chains remaining in the dilute phase [Fig. 2(b)]. We note that this approach works best in the regime where the diffusive timescale  $L_{\rm dil}^2/D_{\rm dil}$  is much smaller than the chain attachment timescale  $\tau$ , where  $L_{\rm dil}$  is half the dimension of the dilute phase normal to the condensate interface. This was found to be the case with  $L_{\rm dil} \sim 0.1~\mu{\rm m}$  and  $D_{\rm dil} \sim 10~\mu{\rm m}^2/{\rm s}$ , so  $L_{\rm dil}^2/D_{\rm dil} \sim$ 1ms and the typical chain attachment timescale  $\tau \sim 10$  ms. Additionally, this survival probability approach was found to be robust to the effect of finite simulation time as compared to directly estimating an average lifetime [Fig. 2(c) and Fig. S2 in the supplementary material].

### III. RESULTS

### A. Effect of client-sticker interaction strength on phase coexistence

We first investigated the effect of both interaction strength and interaction symmetry between the stickers and the client molecules on their phase coexistence. Since sticker beads A and B are thermodynamically identical, clients can either have symmetrically equal interactions with either sticker or preferential interactions with one sticker. For the symmetric case, the interactions of the client with each sticker were set to  $U_{ac} = U_{bc} = \epsilon$ . For the asymmetric case, the preferential interaction  $U_{ac}$  was set to  $2\epsilon$  with  $U_{bc} = 0$  to maintain the same overall interaction energies. For both cases,  $\epsilon$  was systematically varied from 1 to  $4k_BT$  to study the effect of overall interaction strength. As expected, there is a greater degree of client partitioning into the dense phase as the interaction between client and stickers increases. Client concentration in the dense phase increased

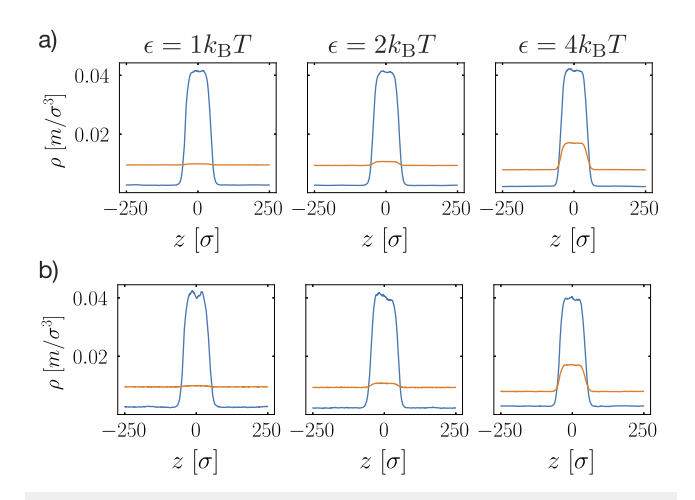


**FIG. 3.** Coexistence density profiles for polymer (blue) and client (orange) species for (a) symmetric and (b) asymmetric interactions. Density profiles were found to be largely invariant with respect to the symmetry of client–sticker interactions.

roughly twofold as the interaction strength was changed from 1 to  $4k_{\rm B}T$  as shown in Fig. 3. The concentration of protein chains in the dense and dilute phases, however, was mostly unaffected, suggesting that the client interaction did not strongly influence the phase separation in the studied regime. A small decrease in dense phase concentration was observed for the highest client interactions, which likely emerges from client–client repulsions due to excluded volume effects. These results highlight that in the client–sticker interaction regime studied, equilibrium phase behavior remains unchanged with client–sticker interaction strength and symmetry.

### B. Effect of client-sticker stoichiometry and interaction strength on chain dynamics

Having established the equilibrium phase coexistence of the model, we then investigated how the presence of client molecules might influence the kinetics of the chain exchange between the dilute and dense phases. Using the approach described previously, we calculated the lifetime of chains in the dilute phase across a range of different client-sticker interaction strengths. We find that as the client-sticker interaction is increased, dilute phase chain lifetimes increase sharply from  $\tau = 8$  ms at  $\epsilon = 1k_{\rm B}T$  to  $\tau = 15$  ms at  $\epsilon = 4k_{\rm B}T$ . Furthermore, we reasoned that the ratio of client to sticker in the system might also influence the dynamics of chain exchange between the phases. To study this effect, we performed simulations of chains at different overall stoichiometries of clients to stickers and calculated the lifetimes of chains in the dilute phase at different interaction strengths (Fig. 4). Surprisingly, we find that overall stoichiometry only has a significant effect at relatively high values of client-sticker interaction. At  $\epsilon = 1k_BT$ , the dilute phase lifetime remains constant as the overall ratio of client to stickers is increased from  $R_{\text{c:s}} = 0.1$  to  $R_{\text{c:s}} = 1$ , while at  $\epsilon = 4k_{\text{B}}T$ , the lifetime increases monotonically as the fraction of client molecules is increased.

To ascertain whether this increase in chain lifetimes within the dilute phase might simply be due to variation in the diffusivity, we calculated the diffusivity of dilute-phase chains as  $\epsilon$  was varied (Table I and Fig. S3 in the supplementary material). We found that the diffusivity followed a nonmonotonic trend with increasing client interaction, with only marginal differences between the symmetric and asymmetric interaction cases. This trend for diffusivity is an emergent effect due to an interplay of the radius of gyration of the chains and the viscosity of the dilute phase (Table I and Fig. S4 in the supplementary material). Thus, changes in diffusivity cannot sufficiently account for the magnitude or sharpness of this change. The only other timescale relevant to the dilute-phase chain lifetime involves the timescale of interfacial attachment. This suggests that

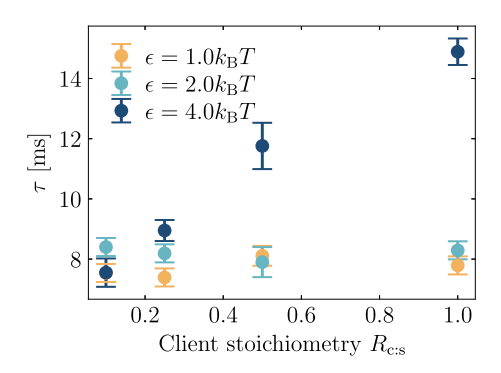


**FIG. 4.** Scaling of dilute-phase chain lifetime with overall client stoichiometry and interaction strength for symmetric interactions. Above a threshold interaction strength, chain lifetimes in the dilute phase were found to increase sharply.

the origin of this effect might lie in the fraction of free stickers available on the incident polymer to associate with those available at the interface.<sup>43</sup> Thus, our findings suggest that above a threshold interaction strength, client molecules increasingly slow down the exchange dynamics between the dilute and dense phases, thereby modulating the condensate dynamics.

### C. Client-sticker interaction symmetry strongly influences exchange dynamics

Our finding that slowing down of chain exchange between dilute and dense phases might emerge from free-sticker sequestration effects in the protein chains led us to probe how the symmetry of the client-sticker interaction influences exchange dynamics. We measured the lifetime of chains across a range of interaction strengths from 1 to  $4k_BT$  for both symmetric and asymmetric interactions between client C and sticker beads A and B, as shown in Fig. 5. Strikingly, we find that for the asymmetric interaction, the dilute-phase chain lifetime is largely unchanged even as the strength of the client interactions is increased. This strong dependence on interaction symmetry for exchange dynamics is distinct from equilibrium properties such as coexistence density and bulk diffusivity of chains. Additionally, we expect that this differential slowing down of chain exchanges also depends on the sequence composition, specifically the relative proportion of A and B stickers. 43 Equal sticker compositions have been shown to lead to low availability of unbound stickers, which would be further enhanced by the presence of clients.<sup>52</sup> Our findings highlight that condensate dynamics are influenced by both the overall energetics and the structure of the

**TABLE I.** Simulated dilute-phase chain lifetimes, dilute-phase diffusivity, radius of gyration, and dimensionless viscosity for symmetric and asymmetric client interactions. Subscript indicates an error on the last digit.

Interaction $(k_{\rm B}T)$	$ au_{ ext{sym}}  ext{ (ms)}$	τ <sub>asym</sub> (ms)	$D_{\text{sym}} (\mu \text{m}^2/\text{s})$	$D_{\rm asym}~(\mu {\rm m}^2/{\rm s})$	R <sub>g,sym</sub> (nm)	R <sub>g,asym</sub> (nm)	$\eta_{ ext{sym}}^*$	$\eta_{ m asym}^*$
1	7.82	7.52	11.4	11.0	3.68	3.66	6.33	6.11
2	8.33	7.83	11.6	12.1	3.66	3.64	$6.0_{2}$	$5.6_{1}$
4	$14.9_{4}$	8.13	9.9	8.2	3.57	3.71	5.31	7.62

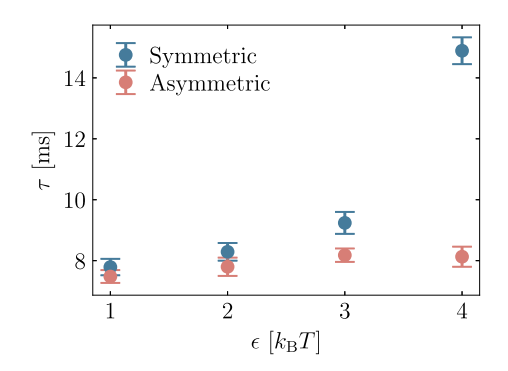


**FIG. 5.** Scaling of dilute-phase chain lifetime with client–sticker interaction strength shows a strong dependence on the symmetry of client–sticker interaction, especially at greater interaction strengths.

interaction network between clients and stickers, in contrast to the coexistence densities.

Next, we investigated the molecular mechanism driving this slowing down of chain exchanges between the dilute and dense phases. Based on our earlier findings, we reasoned that this slowing down of chain exchange dynamics might be linked to changes in the bonding network of the stickers for chains exchanging between the dilute and dense phases. We hypothesized that the symmetric client–sticker interactions would potentially stabilize bound stickers, thereby leading to slowing down of chain exchanges. Quantifying the total fraction of A–B–C clusters, we find that while this quantity predictably increases as the interaction strength is increased, there is almost no dependence on the interaction symmetry (Fig. S5 in the supplementary material). This effect can be attributed to the strong intersticker interactions, resulting in the vast majority of stickers in the dense phase being present as A–B pairs, which interact equivalently with both the symmetric and asymmetric clients.

To obtain a more sensitive metric for ascertaining the cause of slower chain exchange, we calculated the fraction of stickers in our system that were not bound to other stickers (Fig. 6). For chains that have symmetric client interactions, the fraction of unbound stickers in both the dense and dilute phases was found to monotonically decrease with the strength of the client interaction, as expected. In contrast, there was no change in the fraction of unbound stickers for chains with asymmetric client interactions. This is consistent with the trend in chain exchange dynamics where the chains with asymmetric client interactions were found to have dilute-phase chain lifetimes invariant with client interaction strength. Additionally, this data also agrees with our radius of gyration calculations in the dilute phase, which show symmetrically interacting chains having more compact geometries with increasing client interaction, suggestive of more stickers being bound. Thus, our data suggests that the increase in the dilute-phase chain lifetimes for symmetrically interacting stickers arises due to the stabilization of sticker-sticker interactions by the client. This depletes the pool of free stickers available in both phases, therefore hindering the exchange of chains between phases. Taken together, our findings show how both the interaction strength and symmetry of client-sticker interactions can tune the dynamics of transport between phases by stabilizing the lifetime of sticker-sticker bonds.

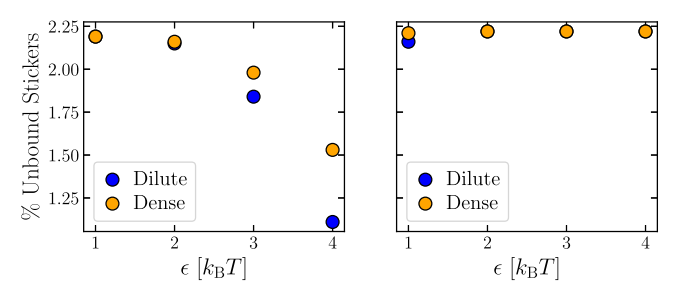


**FIG. 6.** Variation of unbound fraction of stickers as a function of interaction strength for symmetric and asymmetric client interactions.

### IV. CONCLUSION

In this work, we have investigated the exchange dynamics of model protein scaffolds across condensate interfaces in the presence of client molecules. By calculating the dilute-phase chain lifetime distributions, we have systematically elucidated the role of client interactions in chain exchange dynamics. We find that as the strength of client-sticker interaction increases, chains spend longer in the dilute phase. Surprisingly, we also find that there exists a threshold interaction strength beyond which exchange dynamics slow down markedly. While there is a strong linear scaling of the chain lifetime with global client-to-sticker stoichiometry above this threshold interaction, we found almost no dependence below it. These results highlight the important role that client molecules play in modulating the diffusive fluxes across condensate interfaces. We note that this study does not explore the modulatory effects of different classes of client molecules on phase behavior. 48,51,53 In future studies, it would be interesting to explicitly connect the previous investigations on condensate phase equilibria with ligand binding and the scaffold exchange dynamics explored in this work.

Having investigated the role of interaction affinity between clients and stickers, we then asked whether the symmetry of the interaction between the client and the different stickers plays a role. We found that interaction asymmetry does not strongly influence the coexistence densities or the diffusivities in the dilute phase. However, interaction asymmetry was seen to strongly influence the chain exchange dynamics. When the client interacts equally with both stickers, there is a sharp increase in the chain lifetimes, especially beyond a threshold interaction strength. However, when clients interact preferentially with only one type of sticker, this effect is absent. Furthermore, by quantifying the fraction of unbound stickers, we find that as the client-sticker interaction is increased, especially for symmetric interactions, there is a paucity of free stickers in the dense phase. Therefore, chains from the dilute phase are less likely to connect with the dense phase, leading to the slowdown. We note that in our model, client-sticker binding does not change the interactivity of the sticker. In both the symmetric and asymmetric binding cases, client-bound stickers are still capable of interacting with other stickers. However, another biologically relevant scenario is where client binding inhibits the sticker from participating in other sticker-sticker interactions. Future work would examine how the presence of such clients might impact condensate dynamics, especially in different energetic regimes.

Taken together, our findings highlight how biomolecular interaction networks between clients and scaffolds can impact the diffusive fluxes across biological condensates. Depending on their relative interactions, client molecules can sequester sticky residues in scaffolds, thereby slowing down exchange dynamics. Given the recent interest in designing synthetic condensates for metabolic engineering, 54-56 our results highlight the importance of condensate exchange dynamics when considering the rational design of new client–scaffold networks.

### SUPPLEMENTARY MATERIAL

The supplementary material contains additional information on scaling of the exchange timescales with the damping time of the Langevin thermostat y, calculation of finite time effects on chain exchange timescales, diffusivity and viscosity calculations, and dependence of sticker–client–sticker bonding statistics on client–sticker interaction strengths.

#### **ACKNOWLEDGMENTS**

We thank Yaojun Zhang for early help in setting up the model and simulations. This research was primarily supported by the Princeton Center for Complex Materials (PCCM), a U.S. National Science Foundation Materials Research Science and Engineering Center (No. Award DMR-2011750). N.S.W. was supported by NIH Grant No. R01GM140032 and in part by the National Science Foundation, through the Center for the Physics of Biological Function (No. PHY-1734030). Simulations were performed using computational resources provided by the Princeton Institute for Computational Science and Engineering (PICSciE) and the Office of Information Technology's High Performance Computing Center and Visualization Laboratory at Princeton University.

### **AUTHOR DECLARATIONS**

### **Conflict of Interest**

The authors have no conflicts to disclose.

### **Author Contributions**

Ushnish Rana: Conceptualization (equal); Investigation (equal); Writing – original draft (equal); Writing – review & editing (equal). Ned S. Wingreen: Conceptualization (supporting); Funding acquisition (supporting); Writing – review & editing (equal). Clifford P. Brangwynne: Conceptualization (supporting); Funding acquisition (equal); Writing – review & editing (equal). Athanassios Z. Panagiotopoulos: Conceptualization (equal); Funding acquisition (equal); Investigation (equal); Writing – original draft (equal); Writing – review & editing (equal).

### **DATA AVAILABILITY**

The data that support the findings of this study are available from the corresponding author upon reasonable request.

#### **REFERENCES**

- <sup>1</sup>Y. Shin and C. P. Brangwynne, Science 357, eaaf4382 (2017).
- <sup>2</sup>S. F. Banani, H. O. Lee, A. A. Hyman, and M. K. Rosen, "Biomolecular condensates: Organizers of cellular biochemistry," Nat. Rev. Mol. Cell Bio. 18, 285–298 (2017).
- <sup>3</sup>S. Boeynaems, S. Alberti, N. L. Fawzi, T. Mittag, M. Polymenidou, F. Rousseau, J. Schymkowitz, J. Shorter, B. Wolozin, L. Van Den Bosch, P. Tompa, and M. Fuxreiter, Trends Cell Biol. **28**, 420 (2018).
- <sup>4</sup>P. Li, S. Banjade, H. C. Cheng, S. Kim, B. Chen, L. Guo, M. Llaguno, J. V. Hollingsworth, D. S. King, S. F. Banani, P. S. Russo, Q. X. Jiang, B. T. Nixon, and M. K. Rosen, Nature 483, 336 (2012).
- <sup>5</sup>T. S. Harmon, A. S. Holehouse, M. K. Rosen, and R. V. Pappu, Elife 6, e30294 (2017).
- <sup>6</sup>T. J. Nott, E. Petsalaki, P. Farber, D. Jervis, E. Fussner, A. Plochowietz, T. D. Craggs, D. P. Bazett-Jones, T. Pawson, J. D. Forman-Kay, and A. J. Baldwin, Mol. Cell **57**, 936 (2015).
- <sup>7</sup>F. G. Quiroz and A. Chilkoti, Nat. Mater. 14, 1164 (2015).
- <sup>8</sup>S. F. Banani, A. M. Rice, W. B. Peeples, Y. Lin, S. Jain, R. Parker, and M. K. Rosen, Cell **166**, 651 (2016).
- <sup>9</sup>T. S. Harmon, A. S. Holehouse, and R. V. Pappu, New J. Phys. **20**, 045002 (2018).
- M. Rubinstein and A. N. Semenov, Macromolecules 31, 1386 (1998).
   C. P. Brangwynne, P. Tompa, and R. V. Pappu, Nat. Phys. 11, 899 (2015).
- <sup>12</sup>S. Das, Y.-H. Lin, R. M. Vernon, J. D. Forman-Kay, and H. S. Chan, Proc. Natl. Acad. Sci. U. S. A. 117, 28795 (2020).
- <sup>13</sup> J. A. Ditlev, L. B. Case, and M. K. Rosen, J. Mol. Biol. 430, 4666 (2018).
- <sup>14</sup>J. R. Espinosa, A. Garaizar, C. Vega, D. Frenkel, and R. Collepardo-Guevara, J. Chem. Phys. 150, 224510 (2019).
- <sup>15</sup>V. Nguemaha, S. Qin, and H. X. Zhou, J. Phys. Chem. B **122**, 11262 (2018).
- N. W. Sanders, N. Kedersha, D. S. W. Lee, A. R. Strom, V. Drake, J. A. Riback, D. Bracha, J. M. Eeftens, A. Iwanicki, A. Wang, M.-T. Wei, G. Whitney, S. M. Lyons, P. Anderson, W. M. Jacobs, P. Ivanov, and C. P. Brangwynne, Cell 181, 306 (2020).
   Guillén-Boixet, A. Kopach, A. S. Holehouse, S. Wittmann, M. Jahnel, R. Schlüßler, K. Kim, I. R. E. A. Trussina, J. Wang, D. Mateju, I. Poser, S. Maharana, M. Ruer-Gruß, D. Richter, X. Zhang, Y.-T. Chang, J. Guck, A. Honigmann, J. Mahamid, A. A. Hyman, R. V. Pappu, S. Alberti, and T. M. Franzmann, Cell 181, 346 (2020).
- <sup>18</sup> P. Yang, C. Mathieu, R.-M. Kolaitis, P. Zhang, J. Messing, U. Yurtsever, Z. Yang, J. Wu, Y. Li, Q. Pan, J. Yu, E. W. Martin, T. Mittag, H. J. Kim, and J. P. Taylor, Cell 181, 325 (2020).
- <sup>19</sup>J. A. Riback, L. Zhu, M. C. Ferrolino, M. Tolbert, D. M. Mitrea, D. W. Sanders, M.-T. Wei, R. W. Kriwacki, and C. P. Brangwynne, Nature 581, 209 (2020).
- <sup>20</sup>W. Peeples and M. K. Rosen, Nat. Chem. Biol. 17, 693 (2021).
- <sup>21</sup> A. S. Lyon, W. B. Peeples, and M. K. Rosen, Nat. Rev. Mol. Cell Biol. **22**, 215 (2021).
- <sup>22</sup>S. Banjade, Q. Wu, A. Mittal, W. B. Peeples, R. V. Pappu, and M. K. Rosen, Proc. Natl. Acad. Sci. U. S. A. **112**, E6426 (2015).
- <sup>23</sup>D. Zwicker, R. Seyboldt, C. A. Weber, A. A. Hyman, and F. Jülicher, Nat. Phys.
- <sup>24</sup>J. D. Wurtz and C. F. Lee, Phys. Rev. Lett. **120**, 078102 (2018).
- $^{\bf 25}$  A. K. Rai, J.-X. Chen, M. Selbach, and L. Pelkmans, Nature  $\bf 559, 211$  (2018).
- <sup>26</sup>J. Söding, D. Zwicker, S. Sohrabi-Jahromi, M. Boehning, and J. Kirschbaum, Trends Cell Biol. 30, 4 (2020).
- <sup>27</sup>W. M. Jacobs, Phys. Rev. Lett. **126**, 258101 (2021).
- <sup>28</sup> K. Shrinivas and M. P. Brenner, Proc. Natl. Acad. Sci. U. S. A. 118, e2108551118 (2021).
- <sup>29</sup>I. R. Graf and B. B. Machta, "Thermodynamic stability and critical points in multicomponent mixtures with structured interactions," Phys. Rev. Res. 4(3), 033144 (2022).
- <sup>30</sup> A. Z. Lin, K. M. Ruff, F. Dar, A. Jalihal, M. R. King, J. M. Lalmansingh, A. E. Posey, N. A. Erkamp, I. Seim, A. S. Gladfelter, and R. V. Pappu, Nat. Commun. 14, 7678 (2023).
- <sup>31</sup>Y. Dai, C. F. Chamberlayne, M. S. Messina, C. J. Chang, R. N. Zare, L. You, and A. Chilkoti, Chem 9, 1594 (2023).

- <sup>32</sup> M. Linsenmeier, L. Faltova, C. Morelli, U. Capasso Palmiero, C. Seiffert, A. M. Küffner, D. Pinotsi, J. Zhou, R. Mezzenga, and P. Arosio, Nat. Chem. 15, 1340 (2023).
- <sup>33</sup> M. Farag, S. R. Cohen, W. M. Borcherds, A. Bremer, T. Mittag, and R. V. Pappu, Nat. Commun. 13, 7722 (2022).
- <sup>34</sup> M. Farag, W. M. Borcherds, A. Bremer, T. Mittag, and R. V. Pappu, Nat. Commun. 14, 5527 (2023).
- 35 J.-M. Choi, F. Dar, and R. V. Pappu, PLoS Comput. Biol. 15, e1007028 (2019)
- <sup>36</sup>P. Das, S. Matysiak, and J. Mittal, ACS Cent. Sci. 4, 534 (2018).
- <sup>37</sup>G. L. Dignon, W. Zheng, R. B. Best, Y. C. Kim, and J. Mittal, Proc. Natl. Acad. Sci. U. S. A. 115, 9929 (2018).
- <sup>38</sup>G. L. Dignon, W. Zheng, Y. C. Kim, R. B. Best, and J. Mittal, PLoS Comput. Biol. 14, e1005941 (2018).
- <sup>39</sup>J. A. Joseph, A. Reinhardt, A. Aguirre, P. Y. Chew, K. O. Russell, J. R. Espinosa, A. Garaizar, and R. Collepardo-Guevara, Nat. Comput. Sci. 1, 732 (2021).
- <sup>40</sup> U. Rana, K. Xu, A. Narayanan, M. T. Walls, A. Z. Panagiotopoulos, J. L. Avalos, and C. P. Brangwynne, "Asymmetric oligomerization state and sequence patterning can tune multiphase condensate miscibility," Nature Chem. (published online).
- <sup>41</sup>A. Statt, H. Casademunt, C. P. Brangwynne, and A. Z. Panagiotopoulos, J. Chem. Phys. **152**, 075101 (2020).
- <sup>42</sup>U. Rana, C. P. Brangwynne, and A. Z. Panagiotopoulos, J. Chem. Phys. 155, 125101 (2021).

- <sup>43</sup>Y. Zhang, A. G. T. Pyo, Y. Jiang, C. P. Brangwynne, H. A. Stone, and N. S. Wingreen, "Interface resistance of biomolecular condensates," eLife 12, RP91680 (2023).
- <sup>44</sup>N. O. Taylor, M.-T. Wei, H. A. Stone, and C. P. Brangwynne, Biophys. J. 117, 1285 (2019).
- <sup>45</sup> A. Stukowski, Modell. Simul. Mater. Sci. Eng. **18**, 015012 (2009).
- <sup>46</sup>A. G. T. Pyo, Y. Zhang, and N. S. Wingreen, Proc. Natl. Acad. Sci. U. S. A. **120**, e2220014120 (2023).
- <sup>47</sup>J. D. Weeks, D. Chandler, and H. C. Andersen, J. Chem. Phys. **54**, 5237 (1971).
- <sup>48</sup>R. V. Pappu, S. R. Cohen, F. Dar, M. Farag, and M. Kar, Chem. Rev. **123**, 8945 (2023).
- <sup>49</sup>J. A. Anderson, J. Glaser, and S. C. Glotzer, Comput. Mater. Sci. **173**, 109363 (2020).
- <sup>50</sup>J. S. Rowlinson and B. Widom, *Molecular Theory of Capillarity* (Courier Corporation, 2013).
- <sup>51</sup> K. M. Ruff, F. Dar, and R. V. Pappu, Biophys. Rev. **2**, 021302 (2021).
- <sup>52</sup>P. Ronceray, Y. Zhang, X. Liu, and N. S. Wingreen, *Phys. Rev. Lett.* **128**, 038102 (2022)
- <sup>53</sup> K. M. Ruff, R. V. Pappu, and A. S. Holehouse, Curr. Opin. Struct. Biol. 56, 1 (2019).
- <sup>54</sup>D. Bracha, M. T. Walls, and C. P. Brangwynne, Nat. Biotechnol. **37**, 1435 (2019).
- <sup>55</sup>Y. Dai, L. You, and A. Chilkoti, Nat. Rev. Bioeng. 1, 466 (2023).
- <sup>56</sup>M. T. Walls, K. Xu, C. P. Brangwynne, and J. L. Avalos, bioRxiv:2023.10.03.560789 (2023).